



## RESEARCH ARTICLE

Cite this: *RSC Med. Chem.*, 2021, 12, 1540**Multi-target weapons: diaryl-pyrazoline thiazolidinediones simultaneously targeting VEGFR-2 and HDAC cancer hallmarks†**Neha Upadhyay,<sup>a</sup> Kalpana Tilekar,<sup>a</sup> Sabreena Safuan,<sup>b</sup> Alan P. Kumar,<sup>c</sup> Markus Schweipert,<sup>d</sup> Franz-Josef Meyer-Almes <sup>\*d</sup> and Ramaa C S <sup>\*a</sup>

In anticancer drug discovery, multi-targeting compounds have been beneficial due to their advantages over single-targeting compounds. For instance, VEGFR-2 has a crucial role in angiogenesis and cancer management, whereas HDACs are well-known regulators of epigenetics and have been known to contribute significantly to angiogenesis and carcinogenesis. Herein, we have reported nineteen novel VEGFR-2 and HDAC dual-targeting analogs containing diaryl-pyrazoline thiazolidinediones and their *in vitro* and *in vivo* biological evaluation. In particular, the most promising compound **14c** has emerged as a dual inhibitor of VEGFR-2 and HDAC. It demonstrated anti-angiogenic activity by inhibiting *in vitro* HUVEC proliferation, migration, and tube formation. Moreover, an *in vivo* CAM assay showed that **14c** repressed new capillary formation in CAMs. In particular, **14c** exhibited cytotoxicity potential on different cancer cell lines such as MCF-7, K562, A549, and HT-29. Additionally, **14c** demonstrated significant potency and selectivity against HDAC4 in the sub-micromolar range. To materialize the hypothesis, we also performed molecular docking on the crystal structures of both VEGFR-2 (PDB ID: 1YWN) and HDAC4 (PDB-ID: 4CBY), which corroborated the designing and biological activity. The results indicated that compound **14c** could be a potential lead to develop more optimized multi-target analogs with enhanced potency and selectivity.

Received 13th April 2021,  
Accepted 10th June 2021

DOI: 10.1039/d1md00125f

rsc.li/medchem

**Introduction**

Cancer is the most dreaded disease and a major contributor of death worldwide. To battle against cancer, it is imperative to develop an agent with target specificity and potency. Clinical observations suggest that the use of a single-targeting agent might fail to produce the desired therapeutic effects due to development of resistance to the target or mutation.<sup>1</sup> Moreover, the progression of cancer relies on multiple receptors or signaling pathways, and thus, an alternative strategy would be to develop multi-targeting agents.<sup>2</sup> Angiogenesis is known to be involved in cancer progression;<sup>3,4</sup> a variety of factors are involved in regulation of angiogenesis, in which vascular endothelial growth factors

(VEGFs) and their kinase receptors remain the most prominent ones. Tumor cells secrete VEGFs under various conditions such as oncogenic mutations, inflammatory stimuli, hypoxia, stromal and inflammatory cells *etc.* VEGFs interact with their respective VEGF receptors (VEGFRs) which initiates the critical downstream signaling pathway that brings about tumor angiogenesis; thus, targeting VEGFR would be a reasonable therapeutic approach.<sup>5</sup> There are many FDA-approved agents that target VEGFRs (sorafenib, sunitinib, pazopanib, vandetanib, axitinib, regorafenib *etc.*). However, drug resistance is the major concern associated with the monotherapy of these agents;<sup>6,7</sup> hence, over decades researchers have been directing the focus on the potential treatment of resistance.<sup>8</sup> Various dual-targeting agents have been reported in which one target is VEGFR-2 along with other therapeutic targets.<sup>2,9-12</sup> For example, in 2011, using a multitarget approach, cabozantinib was developed as a dual inhibitor of VEGFR-2 and c-Met and used for the treatment of renal cell carcinoma.<sup>13-15</sup>

Though genetics is crucial in cancer progression, epigenetics has become equally important in this field. In the process of epigenetic alterations, histone deacetylases (HDACs) play a key role and therefore become therapeutic targets for anticancer drug discovery.<sup>16,17</sup> HDACs are subdivided into three zinc-dependent classes. Considering

<sup>a</sup> Department of Pharmaceutical Chemistry, Bharati Vidyapeeth's College of Pharmacy, Navi Mumbai, India. E-mail: sinharamaa@yahoo.in<sup>b</sup> Universiti Sains Malaysia School of Health Sciences, Health Campus Universiti Sains Malaysia, 16150 Kubang Kerian, Kelantan, Malaysia<sup>c</sup> Cancer Science Institute of Singapore, Department of Pharmacology, Yong Loo Lin School of Medicine, National University of Singapore, Singapore<sup>d</sup> Department of Chemical Engineering and Biotechnology, University of Applied Sciences, Darmstadt, Germany. E-mail: franz-josef.meyer-almes@h-da.de

† Electronic supplementary information (ESI) available. See DOI: 10.1039/d1md00125f

only human enzymes, class I contains HDACs 1, 2, 3 and 8; class II is subdivided into class IIa consisting of HDACs 4, 5, 7 and 9 and class IIb containing HDAC6 and HDAC10; class IV has only one member, HDAC11. The zinc-dependent HDACs have in common a sequentially and structurally highly conserved active site including a catalytic zinc ion. For the sake of completeness, HDAC class III has also to be mentioned. This special class consists of 7 human members, also named sirtuins, which exploit a different NAD<sup>+</sup>-dependent deacetylation mechanism. Overexpression of HDACs can cause various types of cancers, *e.g.*, colorectal, pancreatic, lung, breast and colon as well as leukemia and hepatocellular carcinoma.<sup>18–22</sup> There is emerging evidence that class IIa HDACs and particularly HDAC4 are involved in cancer.<sup>23,24</sup> One of the best investigated pathways which controls the proliferation of mammary epithelial cells is the MEF2-HDAC axis. Consequently, targeting class IIa HDACs was suggested as a therapeutic strategy for the treatment of breast cancer.<sup>25</sup> Currently, there are five HDAC inhibitors clinically approved as novel antitumor drugs: vorinostat (SAHA), panobinostat (LBH-589), belinostat (PXD-101), romidepsin (FK228) and chidamide. However, their monotherapy fails to display any significant effectiveness against solid tumors<sup>1</sup> and they are associated with various side effects such as thrombocytopenia, leukopenia, diarrhoea, fatigue and potential mutagenicity.<sup>26,27</sup> Mutagenicity is suspected to be associated with hydroxamate zinc binding groups (ZBGs),<sup>28–31</sup> the mechanism being the Lossen rearrangement, a reaction in which hydroxamates are transformed into the corresponding isocyanate.<sup>29</sup> Thus, the best alternative strategy to circumvent mutagenicity would be the development of agents containing non-hydroxamate ZBGs. In addition, there are several mechanisms by which HDAC inhibitors also exhibit anti-angiogenesis activity such as: (1) hypoxia causes expression of HIF-1 $\alpha$  which initiates the transcription of downstream pathways such as overexpression of VEGF,<sup>32</sup> HDAC inhibitors cause suppression of HIF-1 $\alpha$  by initiating the expression of noncoding RNAs that target HIF-1 $\alpha$ <sup>33</sup> and by regulating the transforming growth factor- $\beta$  (TGF- $\beta$ ) pathway,<sup>34–36</sup> leading to anti-angiogenic effects; (2) regulating the acetylation of many non-histone proteins such as P53 which is known to promote degradation of HIF-1 $\alpha$ ;<sup>37,38</sup> (3) tie2-expressing macrophages (TEMs) are known to promote angiogenesis and HDAC inhibitors suppress the M2 polarization of TEMs, thus causing anti-angiogenesis;<sup>39,40</sup> (4) arresting the cell cycle; and (5) apoptosis.<sup>41</sup> Interestingly, one of the mechanisms by which HDACs exert their antitumor effects is downregulation of VEGF<sup>32,42</sup> and suppression of neovascularization through alteration of genes directly involved in angiogenesis.<sup>38,43–45</sup> Thus, using a multitarget approach, selecting VEGFR-2 and HDAC as therapeutic targets for the development of novel dual-targeting agents would offer benefits such as reduced side effects and increased potency.

## Results and discussion

### Designing

The main challenge in designing dual VEGFR-2 and HDAC inhibitors was to achieve a unique framework which satisfied the binding requirements of both targets. In our previous reports, a distinct pharmacophoric drug design was used to achieve both classes of compounds.<sup>46,47</sup> Thus, based on our previous experience with both targets, a multi-targeting strategy was developed by considering VEGFR-2 and HDAC pharmacophore properties.

The pharmacophoric requirement of VEGFR-2 inhibitors are (a) a “hinge-binding” moiety that interacts with the ATP pocket, (b) a “linker” usually comprising 3–5 bond lengths and a hydrogen bond acceptor donor system and (c) a hydrophobic moiety occupying the allosteric site.<sup>48</sup> With these design considerations, we had previously reported 5-benzylidene-2,4-thiazolidinedione analogs as VEGFR-2 inhibitors (Fig. 1;<sup>47</sup> VEGFR-2 IC<sub>50</sub> – 0.5  $\mu$ M). It was hypothesized that a bulky hydrophobic moiety was found to be essential to fill the large empty pocket of the DFG motif;<sup>49,50</sup> thus, we modified the 5-benzylidene-2,4-thiazolidinedione analogs by replacing the terminal aryl group with the bulkier substituted diaryl-pyrazoline (ring A and ring B) and retained the remaining structural features to occlude the basic VEGFR-2 inhibitory activity. Since, pyrazoline-containing compounds have been reported to possess excellent VEGFR-2 inhibition capability<sup>51–55</sup> and antiproliferative potential,<sup>56–59</sup> they were thought to impart antiangiogenic activity to the molecule.

Our above designed structural framework also fits perfectly into the pharmacophoric requirements of HDAC inhibitors. Typical HDAC inhibitors share a broad pharmacophore as a surface recognition cap (SRC) which binds with amino acids of the active site, a hydrophobic linker which occupies the active site channel, and a zinc-binding group (ZBG) which chelates the catalytic zinc ion.<sup>16</sup> The diaryl pyrazoline moiety of our designed molecule was assumed to occupy the cap portion of HDAC, as recent literature highlights pyrazolines as an appropriate surface recognition motif in HDAC inhibitor design.<sup>60–63</sup> Additionally, the literature reports non-classical HDAC inhibitors containing a cyclic ring as a linker rather than a straight hydrocarbon chain;<sup>16,64–66</sup> thus, the central phenyl ring was assumed as a cyclic linker. Several recently reported HDAC inhibitors, the so-called non-hydroxamates, have been an interesting part of the HDAC inhibitors' discovery. In this regard, several non-hydroxamic ZBGs have been identified and reported. On a similar line, in our previously reported HDAC inhibitors, we had incorporated thiazolidinedione (TZD) as a non-hydroxamate ZBG which was found to be an effective antitumor agent (Fig. 1; Mohan *et al.* 2012);<sup>46,66–69</sup> hence, the TZD portion of the currently designed series was assumed as ZBG.

This rational design led to a unique structural framework that could be considered in accordance with the

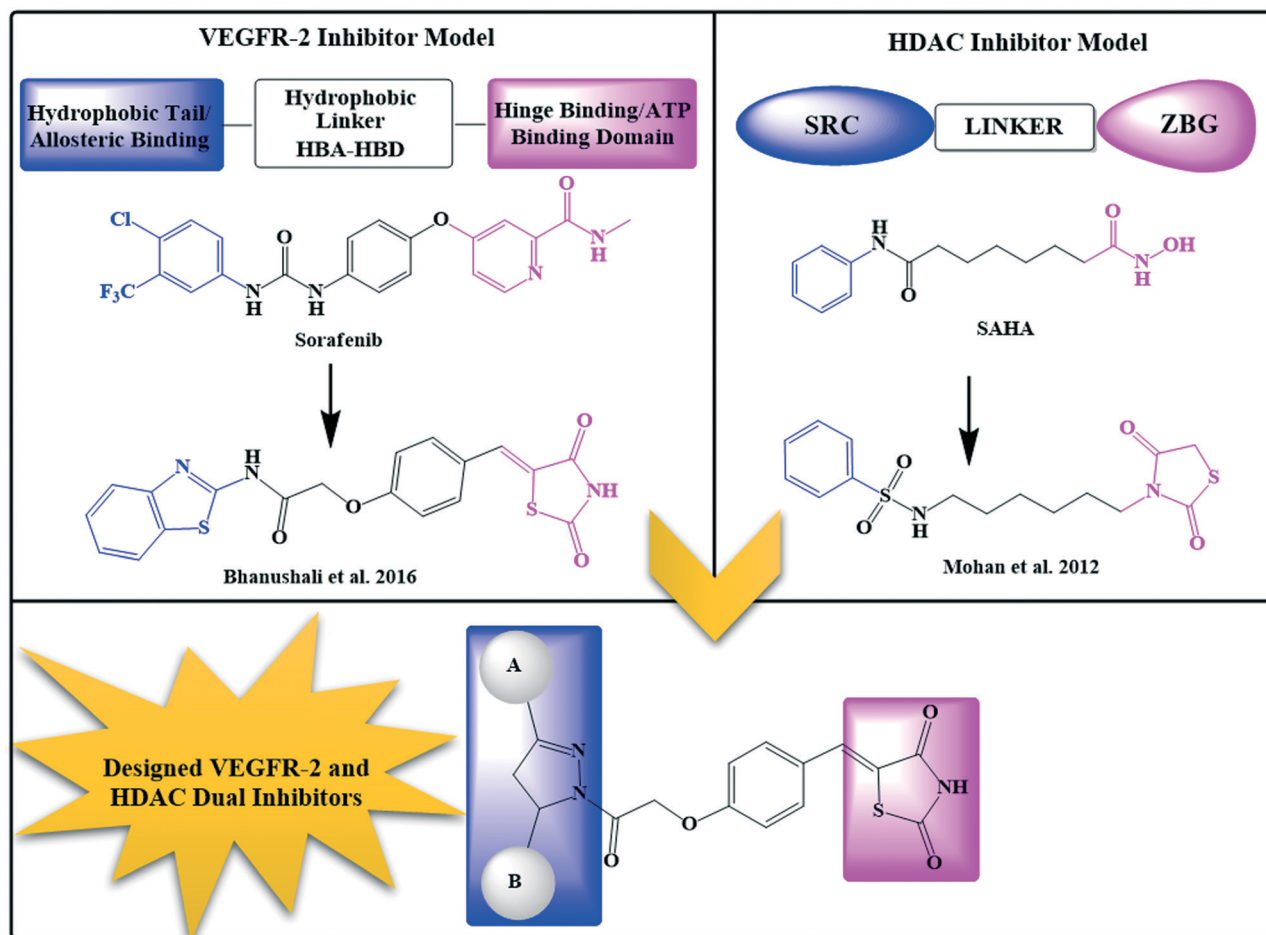


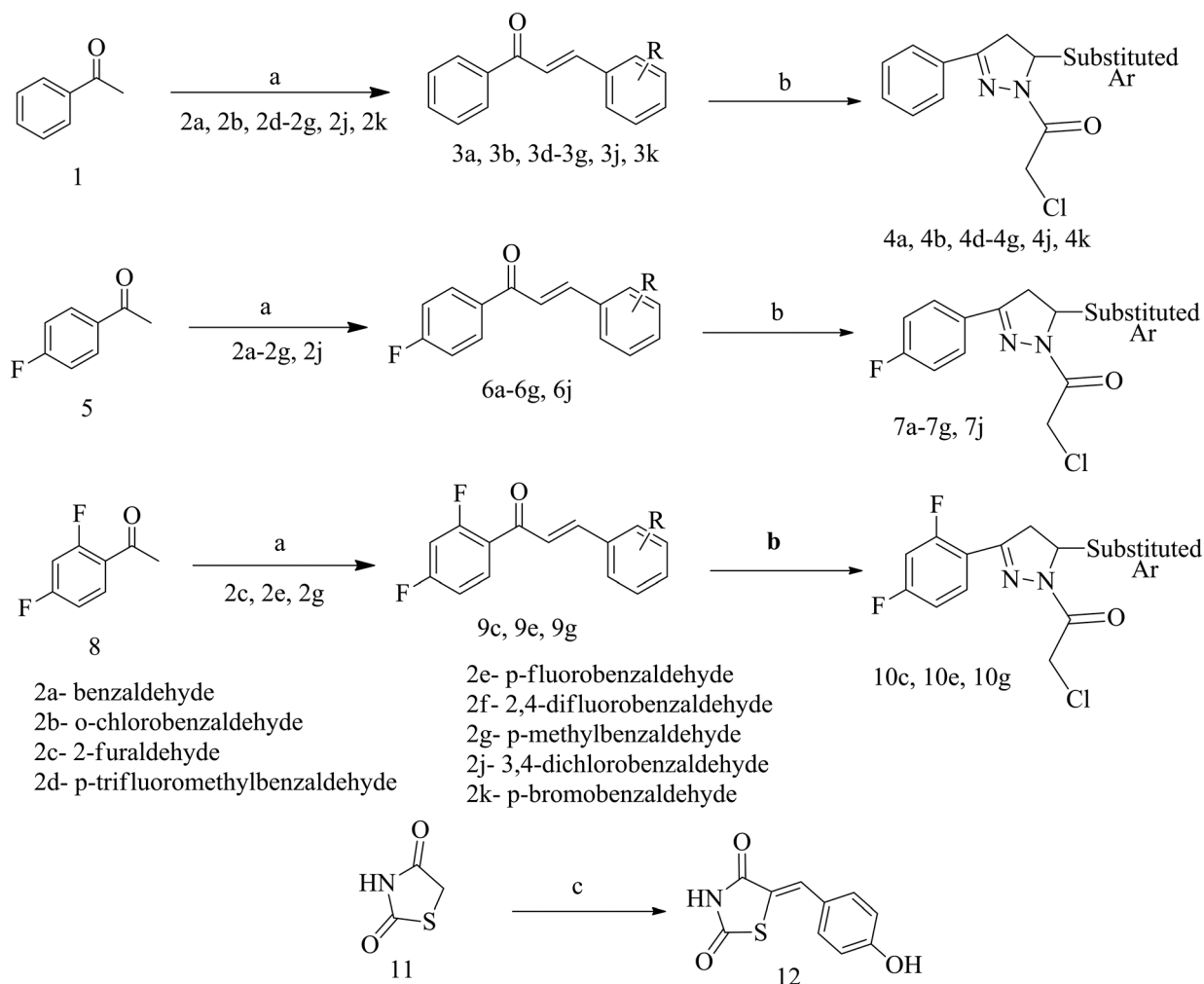
Fig. 1 Rationale of designing novel VEGFR-2 and HDAC dual inhibitors.

pharmacophoric model of both the targets (Fig. 1). The substituted diaryl-pyrazoline group would correspond to the hydrophobic tail of VEGFR-2 and CAP for HDAC. The central phenyl ring with a C=O-CH<sub>2</sub>-O- framework would be the hydrophobic linker for VEGFR-2 and will also function as a cyclic linker of HDAC. The terminal TZD ring would be the hinge binding moiety for VEGFR-2 and ZBG for HDAC. Therefore, we were fairly confident that these compounds could have the capacity to target simultaneously VEGFR-2 and HDAC.

### Chemistry

All the final compounds were synthesized by Schemes 1 and 2. The detailed procedure and spectral observations are presented in the Materials and methods. The purity of all the final compounds, which was >95%, was confirmed by HPLC. All the intermediates were structurally confirmed by <sup>1</sup>H NMR and FTIR spectroscopy, and the final compounds by <sup>1</sup>H NMR, <sup>13</sup>C NMR, FTIR and mass spectrometry. Scheme 1 outlines the synthesis of variously substituted chalcones (3a, 3b, 3d-3g, 3j, 3k, 6a-6g, 6j, 9c, 9e, and 9g), chloroacetylated pyrazolines (4a, 4b, 4d-4g, 4j, 4k, 7a-7g, 7j, 10c, 10e, and 10g) and 5-(4-hydroxybenzylidene)-2,4-thiazolidinedione (12).

The first step was the synthesis of chalcones (3a, 3b, 3d-3g, 3j, 3k, 6a-6g, 6j, 9c, 9e, and 9g) which occurred *via* the renowned Claisen-Schmidt condensation reaction, where different acetophenones (1, 5 and 8) were reacted with substituted aromatic aldehydes (2a-2g, 2j, and 2k) in basic medium to obtain the respective chalcones. The second step involved synthesis of chloroacetylated pyrazoline intermediates (4a, 4b, 4d-4g, 4j, 4k, 7a-7g, 7j, 10c, 10e, and 10g), which proceeded *via* refluxing different chalcones (3a, 3b, 3d-3g, 3j, 3k, 6a-6g, 6j, 9c, 9e, and 9g) with hydrazine hydrate and chloroacetyl chloride in chloroform. The third step was Knoevenagel condensation of 2,4-thiazolidinedione (11) with 2-hydroxybenzaldehyde in the presence of piperidine benzoate in toluene to afford 5-(4-hydroxybenzylidene)-2,4-thiazolidinedione (12). Scheme 2 describes the synthesis of the final compounds (13a, 13b, 13d-13g, 13j, 13k, 14a-14g, 14j, 15c, 15e, and 15g). Reaction of chloroacetylated pyrazolines (4a, 4b, 4d-4g, 4j, 4k, 7a-7g, 7j, 10c, 10e, and 10g) and 5-(4-hydroxybenzylidene)-2,4-thiazolidinedione (12) in DMF and K<sub>2</sub>CO<sub>3</sub> by stirring at RT for 24 h afforded the final compounds (13a, 13b, 13d-13g, 13j, 13k, 14a-14g, 14j, 15c, 15e, and 15g).



**Scheme 1** Synthesis of intermediates. Reagents and conditions: (a) aqueous NaOH, EtOH, RT, 5–6 h; (b)  $\text{NH}_2\text{NH}_2 \cdot \text{H}_2\text{O}$ ,  $\text{CHCl}_3$ , 80 °C, 12 h, then  $\text{K}_2\text{CO}_3$ ,  $\text{ClCH}_2\text{COCl}$ , rt, 12 h; (c) 4-hydroxybenzaldehyde, piperidine benzoate, toluene, reflux, 4 h.

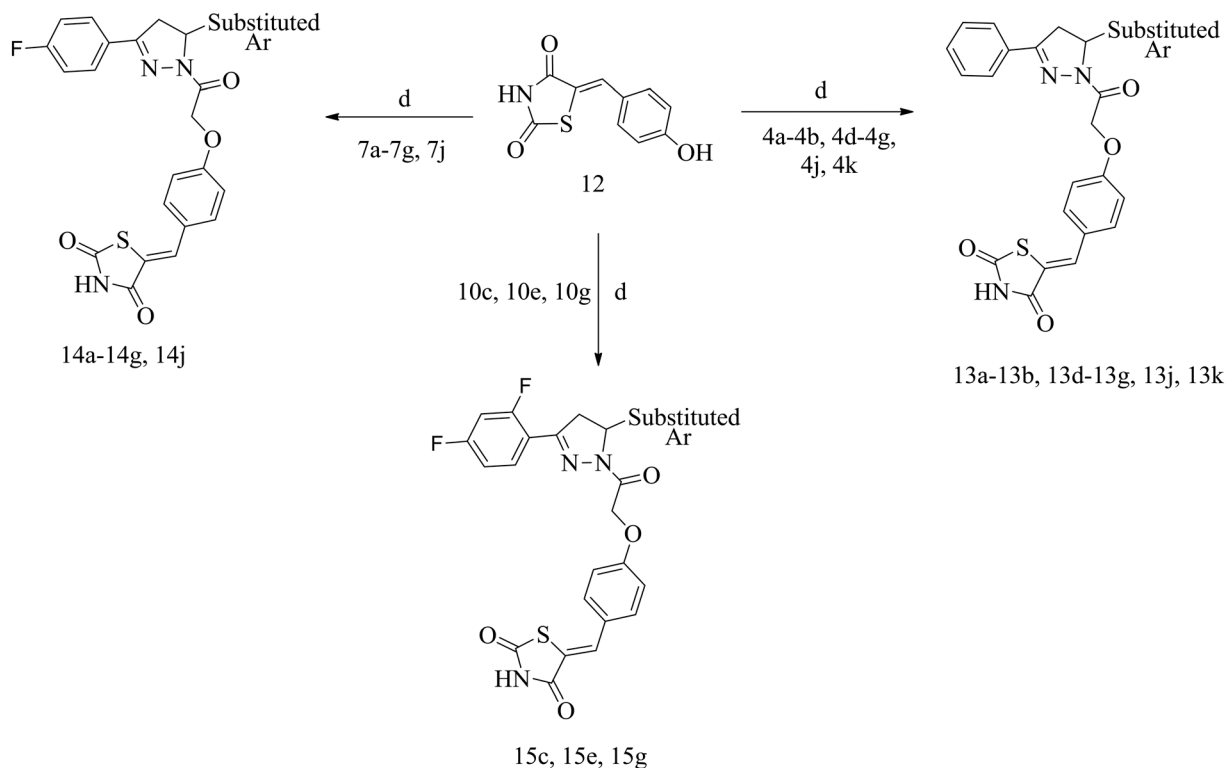
### *In vitro* HDAC enzyme inhibition assay on HDAC4 and HDAC8

To evaluate the HDAC inhibitory potential of all the newly synthesized compounds, an initial *in vitro* screening was performed at 50  $\mu\text{M}$  concentration on HDAC4 (class II) and HDAC8 (class I) and all the compounds showed satisfactory inhibition against both isoforms (Table 1). Compounds with less than 50% residual enzyme activity were evaluated further to determine their inhibitory concentration ( $\text{IC}_{50}$ ); the best compound **13j** showed activity in the sub-micromolar range against HDAC4. Most of the analogs were essentially inactive ( $\text{IC}_{50} > 50 \mu\text{M}$ ) or exhibited 2-digit micromolar  $\text{IC}_{50}$  values against HDAC8. “Cpd16” and “Cpd31” were used as HDAC4 selective reference inhibitors, and the TZD analogs exhibited less potency against HDAC4 than the reference inhibitors.<sup>70,71</sup> In contrast to these reference compounds, the presently reported TZD inhibitors did not contain the zinc-chelating hydroxamate warhead, which mostly contributes to the affinity of classical HDAC inhibitors. Therefore, sub-micromolar activities without typical zinc-chelating groups

appear very promising for the development of HDAC inhibitors with presumably less unwanted toxic effects in later pharmaceutical applications. It is noteworthy that the overall results suggest that the novel diaryl-pyrazoline TZDs exhibit more selectivity and potency towards HDAC4 as compared to HDAC8. Based on the *in vitro* HDAC enzyme inhibition assay results, representative compounds with the most potent inhibitory activity were selected to further determine their anti-angiogenesis capability.

### HDAC selectivity profiling on a panel of HDACs

From the results of the primary evaluation on HDAC4 and HDAC8, compounds **13j**, **14c**, and **14j** were selected for further screening on a panel of HDACs (Table 2) to establish their selectivity profiling on different HDAC isoforms. The assay revealed that **13j** and **14j** were active towards most of the HDAC isoforms; whereas **14c** was more selective towards HDAC4 and its  $\text{IC}_{50}$  was found to be in the sub-micromolar range (Fig. 2). Thus, **14c** could be used as a lead for the development of more optimized molecules and rigorous



**Scheme 2** Synthesis of final compounds. Reagents and conditions: (d)  $K_2CO_3$ , DMF, stirred at RT, 24 h.

**Table 1** Preliminary screening and  $IC_{50}$  determination of pyrazoline-based TZD on HDAC4 and HDAC8 isoforms

Sr. no.	Compounds	Residual HDAC4 activity at 50 $\mu M$ (%)	Residual HDAC8 activity at 50 $\mu M$ (%)	HDAC4 $IC_{50}$ ( $\mu M$ )	HDAC8 $IC_{50}$ ( $\mu M$ )
1	13a	11 $\pm$ 2	39 $\pm$ 1	1.6 $\pm$ 0.2	20 $\pm$ 1
2	13b	14 $\pm$ 1	27 $\pm$ 3	1.2 $\pm$ 0.3	29 $\pm$ 1
3	13d	12 $\pm$ 1	8.2 $\pm$ 0.2	1.0 $\pm$ 0.2	16 $\pm$ 1
4	13e	2.5 $\pm$ 0.5	26 $\pm$ 2	1.7 $\pm$ 0.4	26 $\pm$ 1
5	13f	17 $\pm$ 1	33 $\pm$ 3	2.2 $\pm$ 0.2	34 $\pm$ 10
6	13g	4.6 $\pm$ 0.2	36 $\pm$ 2	1.2 $\pm$ 0.6	31 $\pm$ 1
7	13j	5.9 $\pm$ 0.3	9.4 $\pm$ 1.6	0.7 $\pm$ 0.3	10 $\pm$ 1
8	13k	7.0 $\pm$ 0.6	21 $\pm$ 2	1.2 $\pm$ 2.0	35 $\pm$ 1
9	14a	10 $\pm$ 1	58 $\pm$ 1	4.2 $\pm$ 0.2	>50
10	14b	3.3 $\pm$ 1.3	28 $\pm$ 3	1.1 $\pm$ 0.9	>50
11	14c	36 $\pm$ 2	45 $\pm$ 9	0.88 $\pm$ 4	>50
12	14d	9.2 $\pm$ 1.5	81 $\pm$ 3	1.3 $\pm$ 3	>50
13	14e	3.3 $\pm$ 0.	61 $\pm$ 12	1.4 $\pm$ 0.4	>50
14	14f	10 $\pm$ 2	63 $\pm$ 4	1.6 $\pm$ 0.5	>50
15	14g	10 $\pm$ 1	81 $\pm$ 6	1.8 $\pm$ 0.4	>50
16	14j	13 $\pm$ 2	22 $\pm$ 3	0.8 $\pm$ 0.2	25 $\pm$ 7
17	15c	22 $\pm$ 3	100 $\pm$ 8	15 $\pm$ 2	>50
18	15e	10 $\pm$ 4	69 $\pm$ 5	1.5 $\pm$ 0.7	>50
19	15g	9.4 $\pm$ 1.8	69 $\pm$ 3	1.5 $\pm$ 0.2	>50
20	Cpd 16 (ref. 72)	—	—	0.039	6.7
21	Cpd 31 (ref. 73)	—	—	0.02	0.36

structural modifications could provide analogs with enhanced potency and efficacy towards HDAC4 isoforms in the future.

**Thermal shift assay on HDAC4.** Thermal shift is used to demonstrate target engagement (TE) by a ligand. Binding of a ligand to the target protein can shift the melting temperature of the protein to the higher or lower side as

compared to free protein, thus producing a thermal shift. Test compounds with HDAC4 inhibitory potential (13j and 14j) were subjected to this assay with the HDAC4 isoform to examine the thermal stabilization of the ligands. The melting temperature of free HDAC4 (DMSO control) was 57.3  $^{\circ}C$ , and those of the protein in the presence of the test compounds were 56.7  $^{\circ}C$  and 57.3  $^{\circ}C$  for 13j and 14j, respectively (Fig. 3).

**Table 2** Selectivity profile of pyrazoline-based TZD inhibitors against a panel of human HDACs. IC<sub>50</sub> values are means, and errors were obtained from statistical analysis of non-linear regression fits to sets of 10 data points

IC <sub>50</sub> (μM)							
Compound	HDAC1	HDAC2	HDAC3	HDAC4	HDAC6	HDAC7	HDAC8
13j	4.9	13	9.1	0.7 ± 0.3	39	>50	10 ± 1.0
14c	>50	>50	>50	0.88 ± 4	7.6	>50	>50
14j	11	21	11	0.8 ± 0.2	13	6.7	25 ± 7.0

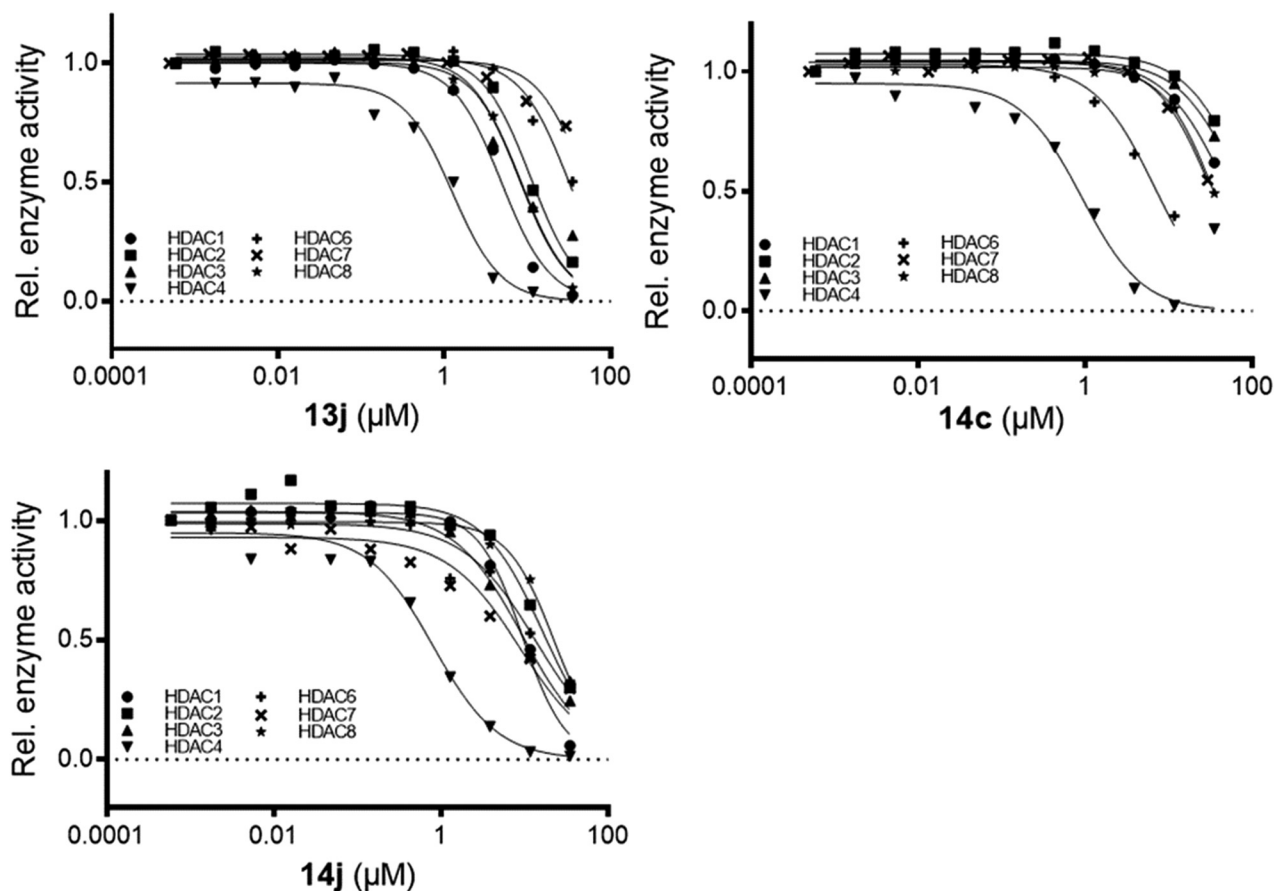


**Fig. 2** Dose-response curve of compounds 13j, 14c, and 14f on different HDAC isoforms.

These minor changes in comparison with the melting point of the unbound enzyme were within the error range of the method. Altogether, even though the compounds were able to inhibit HDAC4 in sub-micromolar concentrations, they contribute nothing or only to a minor degree to protein stabilization.

#### Cytotoxicity assessment on HUVEC proliferation

Human umbilical vein endothelial cells (HUVECs) are the most commonly used human endothelial cells for *in vitro* angiogenesis assays.<sup>74,75</sup> In the development of sprouting angiogenesis, endothelial cells undergo proliferation, which is related to survival of new vessels; thus, the effects of anti-angiogenic agents on the proliferation of HUVECs

could be measured by the MTT assay,<sup>74-77</sup> in which the number of viable cells is determined. Nine compounds with the highest HDAC4 inhibition potential (13b, 13d, 13j, 14a, 14c-14e, 14j, and 15g) were selected to determine their *in vitro* cytotoxicity effects on HUVEC proliferation. STS was used as a positive control. Five different concentrations (10, 1, 0.1, 0.01, and 0.001 μM) of test compounds as well as the positive control were used to determine their inhibition potential. Results showed that compounds 13b, 14c, 14d and 14j exhibited satisfactory inhibition effects on HUVEC proliferation (IC<sub>50</sub> <10 μM), while 13d, 13j, 14a, 14e and 15g displayed poor inhibition (>10 μM). Moreover, 14c showed inhibitory activity comparable to that of STS (Table 3); thus, we assume that it may have potential anti-angiogenic activity.

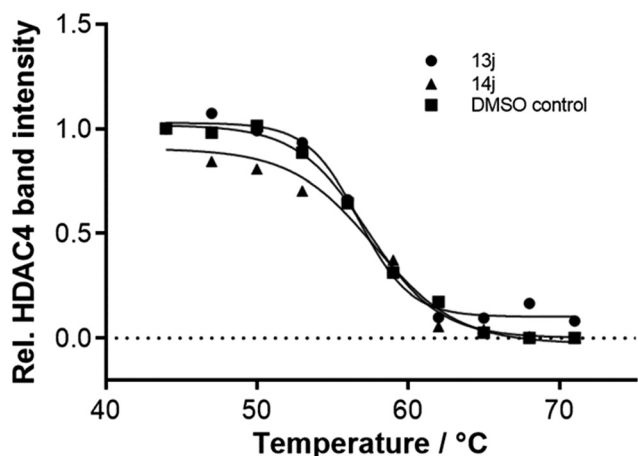


Fig. 3 Thermal stabilization of 3  $\mu\text{M}$  HDAC4 upon binding of 100  $\mu\text{M}$  13j and 14j.

### VEGFR-2 inhibition assay

Test compounds with inhibitory capability on HUVEC proliferation (13a, 14c, 14d, and 14j) were selected to determine their effects on the activity of VEGFR-2 phosphorylation, which is known to activate other signalling cascades associated to endothelial cells and bring about proliferation, migration, invasion, and cell differentiation.<sup>78,79</sup> An *in vitro* cell-based ELISA method was used in which all four test compounds along with the positive control STS were preliminarily tested at 10  $\mu\text{M}$  concentration against pVEGFR-2. The test compounds with noticeable structural differences displayed poor to good % VEGFR-2 inhibition, wherein 14c showed >50% inhibition, and the  $\text{IC}_{50}$  of 14c further confirmed its pVEGFR-2 inhibition potential. Structurally, 14c contains 4-fluorophenyl

Table 4 VEGFR-2 inhibitory activity of 13a, 14c, 14d, and 14j

Sr. no.	Code	% Inhibition <sup>a</sup> (at 10 $\mu\text{M}$ )	$\text{IC}_{50}$ ( $\mu\text{M}$ )
1	13b	48.95	ND <sup>b</sup>
2	14c	56.66	5
3	14d	48.71	ND <sup>b</sup>
4	14j	22.36	ND <sup>b</sup>
5	STS <sup>c</sup>	87.85	0.5

<sup>a</sup> Assays were performed in replicate ( $n \geq 2$ ). <sup>b</sup> Not determined. <sup>c</sup> STS represents staurosporine.

at ring A and 2-furyl at ring B, while the other two compounds with 4-fluorophenyl at ring A (14d and 14j) and other substituents at ring B (14d: 4-trifluoromethylphenyl; 14j: 3,4-dichlorophenyl) displayed <50% inhibition (Table 4). However, compound 14j exhibited a remarkable decrease in % VEGFR-2 inhibitory activity as compared to 14c and 14d, which suggested that dichlorophenyl at ring B is of least preference as compared to the other substituents.

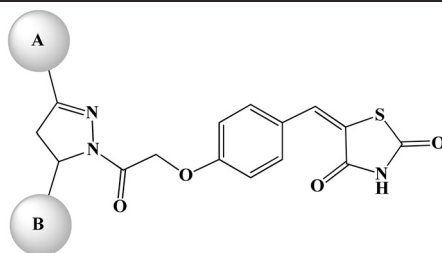
### Molecular docking study

A complete docking study was performed to predict the binding pose of the ligand and determine the putative molecular determinants of protein–ligand binding. The docking procedure was validated by redocking of the ligand in the crystal structure of VEGFR-2 (PDB-ID: 1YWN) and HDAC4 (PDB-ID: 4CBY).<sup>70</sup> The ligands were docked into the protein receptor which yielded an almost perfect overlap with the X-ray pose (ESI<sup>†</sup>). Thus, by assuming that all parameters were well configured for docking of pyrazoline TZD analogs, the same crystal structures were used throughout the docking study. The GBVI/WSA dG docking score of the redocked ligand was  $-11.2$  on VEGFR-2 and  $-13.6$  on HDAC4

Table 3  $\text{IC}_{50}$  of HUVECs by compounds 13b, 13d, 13j, 14a, 14c–14e, 14j, and 15g

Sr. no.	Code	$\text{IC}_{50}$ <sup>a</sup> ( $\mu\text{M}$ )	A ring	B ring
1	13b	2	Phenyl	2-Cl phenyl
2	13d	>10	Phenyl	4- $\text{CF}_3$ phenyl
3	13j	>10	Phenyl	3,4-DiCl phenyl
4	14a	>10	4-F phenyl	Phenyl
5	14c	0.7	4-F phenyl	2-Furyl
6	14d	6	4-F phenyl	4- $\text{CF}_3$ phenyl
7	14e	>10	4-F phenyl	4-F phenyl
8	14j	2	4-F phenyl	3,4-DiCl phenyl
9	15g	>10	2,4-DiF phenyl	4-Tolyl
10	STS	0.5	—	—

<sup>a</sup> Assays were performed in replicate ( $n \geq 2$ ).



(ESI<sup>†</sup>). Docking of the complementary stereoisomers of **14c** and **14j** showed similar binding poses of (*S*)-**14c**, (*R*)-**14j** and (*S*)-**14j** having the same absolute configuration at the pyrazole ring (ESI<sup>†</sup>). The binding mode of (*S*)-**14c** to VEGFR-2 resembles that of previously reported TZD analogs.<sup>47</sup> The TZD warhead forms two hydrogen bonds with L838 and A1048. Multiple hydrophobic pi-alkyl and alkyl interactions contribute further to affinity (Fig. 4).

Furthermore, the docking study of compounds **14c** and **14j** with HDAC4 gained more insight into the mode of molecular interaction. The results for the two enantiomers of these analogs show rather similar docking scores, which were considerably lower than that obtained from redocking the reference compound “Cpd 31” into the crystal structure of its complex with the catalytic domain of HDAC4 (Fig. 5).<sup>71</sup> This appears realistic, since “Cpd 31” is about 45-fold more active against HDAC4 than **13d** and **14c** (Table 1). Looking closer at the binding pose of (*S*)-**14c**, it was revealed that the TZD group was able to replace the hydroxamate warhead of classic HDAC inhibitors, since the TZD group not only interacted with the catalytic zinc ion in the catalytic site but also showed amide- $\pi$  stacking with G811 and  $\pi$ -alkyl interaction with L943 (Fig. 5). The binding was also strengthened by parallel  $\pi$ -stacking interactions with F871. The branched pyrazoline group serving as capping group was largely exposed to the surrounding solvent but showed an amide- $\pi$  interaction with F870. Therefore, it is not unexpected that different substitution patterns at the aromatic rings of the capping group have no big influence on the enzyme inhibitory activity (ESI<sup>†</sup>). Thus, the docking results confirmed that the pyrazoline TZD analogs of this study were biologically active against both target proteins VEGFR-2 and HDAC4.

### Endothelial cell migration assay

Endothelial cell mobility is significant for tumor angiogenesis which is known to be initiated by different

growth factors.<sup>80,81</sup> To measure the extent of endothelial cell motility against test compounds, scrape wound healing assay was performed. The migration capability of HUVECs was determined for the most active compound **14c** along with positive control STS, which was measured in percent wound healing. As compared to untreated HUVECs, STS-treated HUVECs suppressed the endothelial cell migration to a greater extent (Fig. 6). The inhibitory effect of **14c** on the mobility of HUVECs was less than that of STS but greater than that of untreated, evident by percent wound healing. Thus, with the results it was clear that **14c** has the potential to interfere with the migration capability of endothelial cells.

### Capillary tube formation assay

The process of angiogenesis requires capillary-like tube formation of endothelial cells for ease of blood flow, and it is considered as representative of later stages of angiogenesis. Thus, the tube formation assay is extensively used to determine the *in vitro* anti-angiogenic effects of test compounds.<sup>74–77</sup> Compound **14c** exhibited substantial inhibition of HUVEC proliferation, VEGFR-2 phosphorylation, and migration; thus, it was further evaluated to determine its effect on the tube formation capability of HUVECs. After 24 h, STS-treated HUVECs reduced the number of capillaries to a greater extent as compared to untreated which formed hollow capillary-like structures (Fig. 7A and B). However, **14c** did not significantly decrease the capillary formation in comparison with STS (Fig. 7C and Table S2<sup>†</sup> ( $p = 0.31$ )). Thus, we could state that **14c** has less potential to decrease the tube formation activity of HUVECs as compared to STS.

### MTT cytotoxicity assay

Considering *in vitro* results of anti-angiogenic assays, **14c** was evaluated for its effects on the cytotoxicity of four different cancer cell lines: MCF-7 (human breast cancer), K562 (leukaemia), A549 (human lung cancer), and HT-29 (human

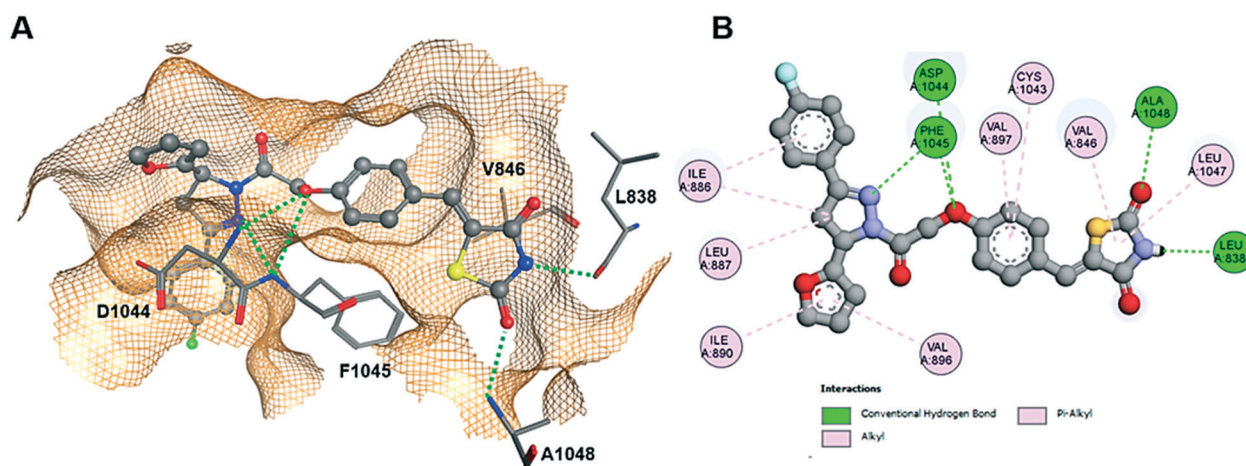


Fig. 4 Docking of (*S*)-**14c** into VEGFR-2. (A) 3D binding pose showing hydrogen bonds (dotted green lines) to L838 and A1048. (B) Detailed 2D protein-ligand interactions.



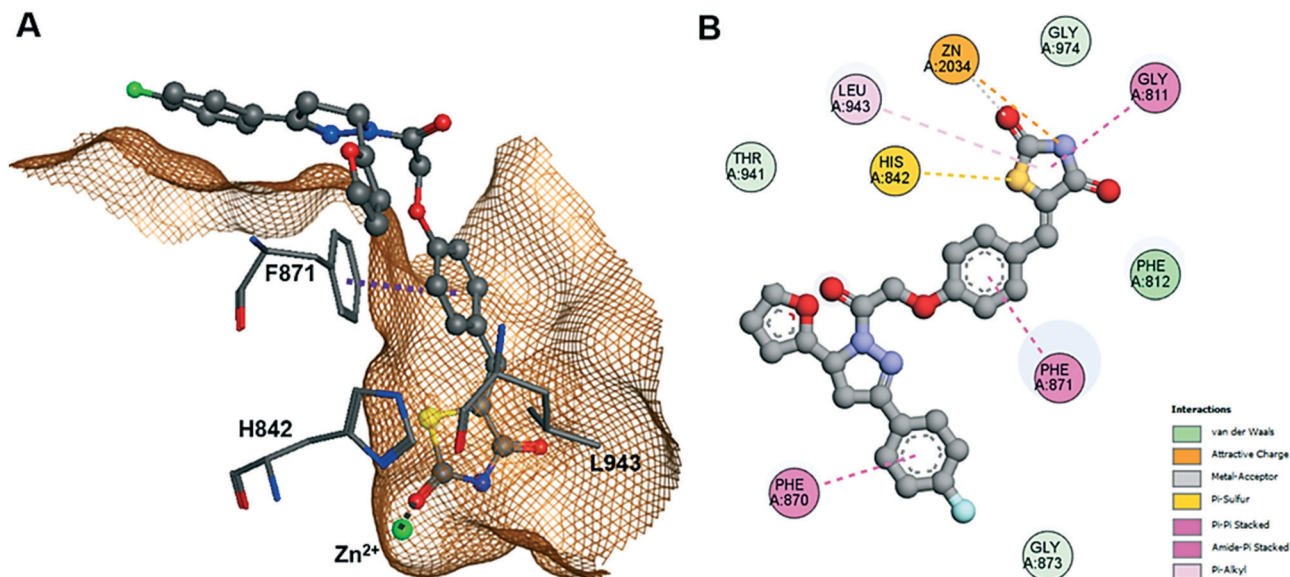


Fig. 5 Docking pose of (S)-14c in the active pocket of HDAC4 (PDB-ID: 4CBY). (A) 3D binding pose showing hydrogen bonds with F871 and Zn<sup>2+</sup> interaction. (B) Detailed 2D protein-ligand interactions.

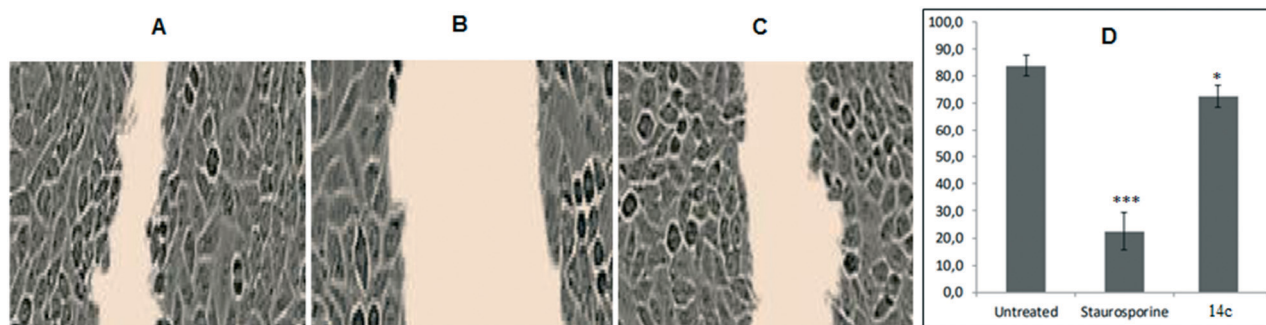


Fig. 6 (A–C) Representative images of cellular migration assay in HUVECs after 8 h of untreated, STS (10 μM mL<sup>-1</sup>), and 14c (10 μM mL<sup>-1</sup>), respectively. (D) Graphical representation of percent wound healing. Error bars represent SEM,  $n = 3$ , \* $p \leq 0.01$ ; \*\*\* $p \leq 0.0001$  (compared to untreated; calculated with unpaired Student's  $t$ -test).

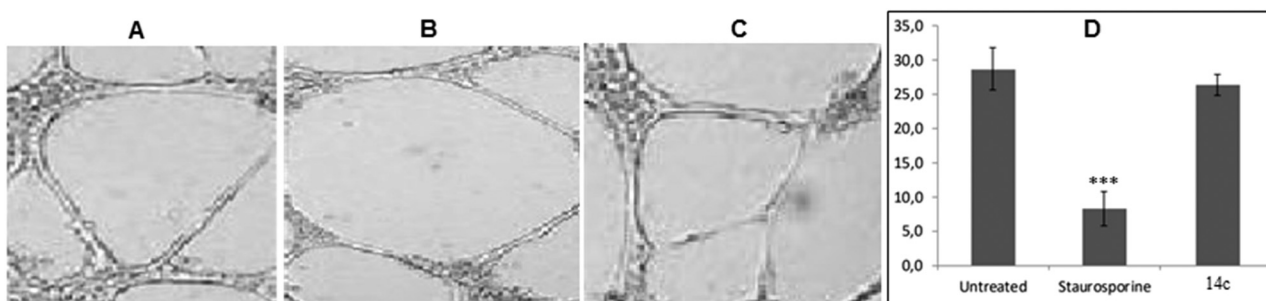


Fig. 7 (A–C) Images of HUVEC capillary-like tube formation assay after 48 h of untreated, STS (10 μM mL<sup>-1</sup>), and 14c (10 μM mL<sup>-1</sup>), respectively. (D) Graphical representation of intersection counts with different treatments. Error bars represent SEM,  $n = 3$ , \*\*\* $p \leq 0.0001$  (STS compared to untreated; calculated with unpaired Student's  $t$ -test).

colorectal adenocarcinoma). Results revealed that 14c exhibited moderate to good cytotoxicity on these four cancer cell lines (Table 5). The positive control paclitaxel was several fold more potent than 14c, whereas cisplatin showed

variation in activity. HT-29 cell lines appeared to be most affected by 14c followed by A549, MCF-7 and K562 (ESI<sup>†</sup>). Thus, we assume that 14c has potential cytotoxicity against these cancer cell lines.

**Table 5** Cancer cell viability of **14c**

Compound	IC <sub>50</sub> <sup>a</sup> (μM)			
	MCF-7	K562	A549	HT-29
<b>14c</b>	28.41 ± 4.2	46.27 ± 1.6	19.52 ± 1.44	18.84 ± 1.1
Paclitaxel	0.35	0.29	0.32	0.28
Cisplatin	10.57 ± 1.1	58.4 ± 1.4	16.68 ± 1.74	10.6 ± 1.2

<sup>a</sup> Assays were performed in replicate ( $n \geq 2$ ).

**In vivo chick chorioallantoic membrane (CAM) assay.** The CAMs are easy to access outside the embryo and represent a reliable approach to study the anti-angiogenic effects of compounds *in vivo*.<sup>77</sup> Compound **14c** was chosen to evaluate its inhibitory effects on growing CAMs to confirm the *in vivo* anti-angiogenic activity. After 12 days of implanting sponges loaded with the test compound into the CAMs, the average number of blood vessels was determined. It was observed that untreated CAMs were surrounded by allantoic vessels with newly formed capillaries (Fig. 8A), whereas **14c**-treated (Fig. 8B) CAMs demonstrated significant reduction in the number of branching of capillaries, further supporting its anti-angiogenic effects.

## Materials and methods

### Chemistry

All the reagents, solvents, chemicals *etc.* were procured from sources, *viz.* Sigma Aldrich, S.D. Fine Chem. Ltd., and Himedia, and utilized without any further purification. The reactions were monitored at each step by thin layer chromatography (TLC) using Merck precoated silica gel 60 F-254 plates under short wave UV light (254 nm) to identify the UV absorbing spots for completion of the reaction and also to trace any impurities. All intermediates were purified by a recrystallization method using suitable solvents such as chloroform, methanol *etc.* All the final molecules were purified by a column chromatography technique on silica gel 60 (60 to 120 mesh) using a suitable combination of different solvents. The melting points of all the intermediates were obtained by using a VEEGO model VMP-DS melting point

apparatus and those of the final compounds were obtained using a DSC1 STAR system differential scanning calorimeter from Mettler Toledo. The purity of all final compounds was determined using an Agilent 1200 high-performance liquid chromatography (HPLC) system with the software EZ chrome Elite. The chromatographic column used was HemochromIntsil A31 C18 5U 150 mm × 4.6 mm Sn-B180127, detection at 300 nm. A UV-visible detector was used with a flow rate of 1 mL min<sup>-1</sup>. The oven temperature was maintained at 30 °C; gradient elution with a run time of 10 min using methanol:formic acid (1%) (formic acid: in 1000 mL double-distilled water 1 mL formic acid was added) in an 80:20/90:10 ratio. The structures of intermediates were confirmed by FTIR and <sup>1</sup>H NMR and that of the final compounds by FTIR, <sup>1</sup>H NMR, <sup>13</sup>C NMR and mass spectrometry. IR analysis was performed using a JASCO FT/IR-4100 type A spectrometer using a manual sampling method. <sup>1</sup>H NMR spectra were recorded using a Bruker Avance 400 MHz spectrometer with DMSO-*d*<sub>6</sub>. All shifts are reported in δ (ppm) units relative to the signals for solvent DMSO (δ - 2.50 ppm). All coupling constants (*J* values) are reported in hertz (Hz). NMR abbreviations are bs, broad singlet; s, singlet; d, doublet; t, triplet; q, quartet; m, multiplet; and dd, doublet of doublets. <sup>13</sup>C NMR was recorded on a Bruker Avance spectrometer at 100 MHz with DMSO-*d*<sub>6</sub>. The mass spectrum was determined on an LC-MS Agilent Technologies 1260 Infinity instrument. All final compounds were synthesized by Schemes 1 and 2. Scheme 1 represents the synthesis of intermediates and Scheme 2 of the final compounds.

### Procedure for synthesis of chalcone intermediates

Different chalcones were synthesized using a previously reported procedure<sup>82,83</sup> with some minor modifications. In short, to ethanolic NaOH solution (10%, 20 mL), different acetophenones (0.04 mol-acetophenone, 4-fluoroacetophenone, and 2,4-difluoroacetophenone) were added followed by aldehydes (0.04 mol **2a-2g**, **2j**, and **2k**) in an ice bath and stirred at room temperature (RT) for 5–6 h. The solid precipitate was filtered and washed with cold water. It was then

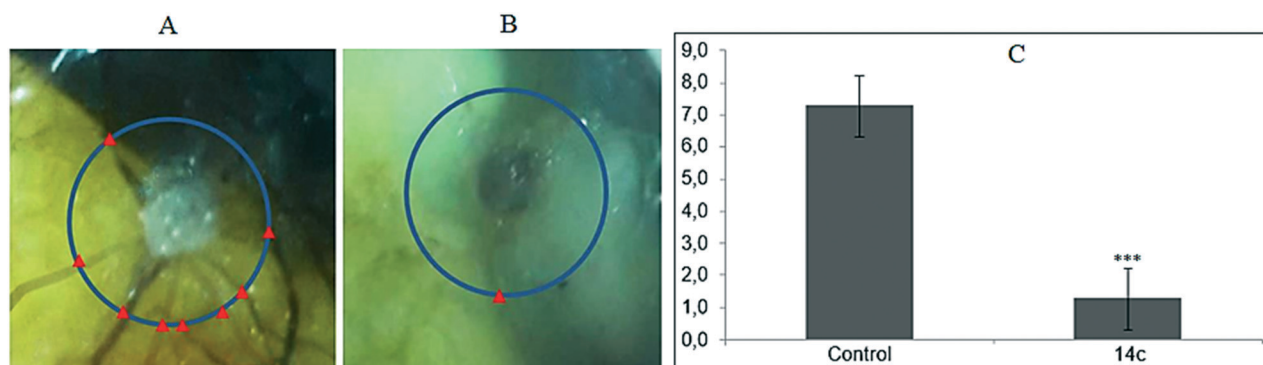


**Fig. 8** Representative images of untreated (A) and **14c**-treated (B) CAMs. (C) Graphical representation of CAM assay. Error bars represent SEM,  $n = 4$ , \*\*\* $p \leq 0.0001$  (STS compared to untreated; calculated with unpaired Student's *t*-test).

recrystallized with ethanol to obtain the appropriate chalcones (**3a**, **3b**, **3d–3g**, **3j**, **3k**, **6a–6g**, **6j**, **9c**, **9e**, and **9g**) (Scheme 1).

#### Procedure for synthesis of chloroacetylated pyrazoline intermediates

Various pyrazole derivatives were synthesized and previously reported by us.<sup>82,83</sup> With minor modifications in the previous procedure, we synthesized pyrazoline derivatives from their respective chalcones. To a solution of chalcones (**3a**, **3b**, **3d–3g**, **3j**, **3k**, **6a–6g**, **6j**, **9c**, **9e**, and **9g**) (0.02 mol) in chloroform, hydrazine hydrate (0.04 mol) was added and refluxed for 12 h. In this reaction mixture  $K_2CO_3$  (0.05 mol) was added and stirred for 15 min followed by chloroacetyl chloride (0.03 mol) with stirring under an ice bath and stirred at RT. After 12 h the reaction was stopped, and the chloroform layer was washed with water to remove excess  $K_2CO_3$  and evaporated to obtain the solid. The crude was purified by extracting with diethyl ether to obtain the appropriate chloroacetylated pyrazoline intermediates (**4a**, **4b**, **4d–4g**, **4j**, **4k**, **7a–7g**, **7j**, **10c**, **10e**, and **10g**) (Scheme 1).

#### Procedure for synthesis of 5-(4-hydroxybenzylidene)-2,4-thiazolidenedione (12)

Intermediate 12 was synthesized using a previously reported procedure,<sup>84,85</sup> in which 2,4-thiazolidenedione (4.68 g, 0.04 mmol) and 4-hydroxy benzaldehyde (4.88 g, 0.04 mmol) were dispersed in toluene followed by a catalytic amount of piperidinium benzoate and this reaction mixture was refluxed in a Dean Stark apparatus for 4 h. The reaction mixture was cooled to RT and the solid precipitated out was collected by vacuum filtration to obtain 12 (Scheme 1). Yellow solid. Yield 11 g (89%). M. P. 300–302 °C.

#### Procedure for synthesis of final compounds

The target compounds were synthesized using a similar synthetic route mentioned previously.<sup>66,85</sup> 5-(4-Hydroxybenzylidene)-2,4-thiazolidenedione (**12**) (1.0 mol) and potassium carbonate ( $K_2CO_3$ ) (1.5 mol) were added to dimethyl formamide (DMF) (10 mL) and stirred for 5 min at RT. To this solution chloroacetylated pyrazolines (**4a**, **4b**, **4d–4g**, **4j**, **4k**, **7a–7g**, **7j**, **10c**, **10e**, and **10g**) (1.5 mol) were added and stirred for 24 h at RT. The reaction was quenched by adding water (50 mL); the precipitated solid was collected by filtration and washed with water. The crude was purified by column chromatography with hexane:ethyl acetate (1:1 to 1.5:0.5) solvent to obtain the final products (**13a**, **13b**, **13d–13g**, **13j**, **13k**, **14a–14g**, **14j**, **15c**, **15e**, and **15g**) (Scheme 2).

The ESI<sup>+</sup> contains all the characterization data.

#### HDAC enzyme inhibition assay

Recombinant HDAC1, 2, 3, 6 and 7 were purchased from BPS Bioscience. Recombinant HDAC8 was produced as described recently.<sup>86</sup> In short, HDAC8 was produced in *E. coli* (BL21)

DE3 pLysS cells using a pET14b vector containing codon-optimized human HDAC8. The expression of recombinant cHDAC4 was performed according to another recently published procedure.<sup>87</sup> Recombinant cHDAC4 was expressed in *E. coli* (BL21) DE3 pLysS using a pET14b vector (Novagen, EMD Millipore) containing the codon-optimized catalytic domain of human HDAC4, fused to an N-terminal His6-SUMO tag and a C-terminal SII tag and auto-induction medium. Enzyme activity assays were performed in a two-step procedure as described in detail previously.<sup>87</sup> The fluorogenic activity assay relies on the transformation of Boc-Lys(trifluoroacetyl)-AMC (Bachem) as substrate for HDAC4, 7 and 8 and Boc-Lys(acetyl)-AMC as substrate for HDAC1, 2, 3 and 6. Afterwards, the deacetylated substrates are converted into a fluorescent product by trypsin.

#### Thermal shift assay of HDAC4

HDAC4 was tested in the absence (DMSO control) and in the presence of the compounds. For the thermal shift assay, 3  $\mu$ M HDAC4 was mixed with 100  $\mu$ M of compound (dissolved in DMSO) and incubated for 15 min at 30 °C. Ten aliquots of this mix were transferred into PCR strips (25  $\mu$ l per well) and further incubated for 60 min at 30 °C in a PCR cycler (T Gradient, Biometra). Each indicated temperature was held for 10 min followed by a temperature increase of 2 °C. After 9.5 min, a sample from the respective well was stored on ice. After the sample collection for all indicated temperatures, the samples were centrifuged at 4 °C and 18000g for 15 min. After centrifugation the supernatant was treated with Laemmli buffer and denatured *via* heat followed by SDS-PAGE. By using ImageJ program, the relative band intensity at each indicated temperature was calculated, and the GraphPad Prism program was used for plotting intensities against respective temperatures and fitting the data to a logistic function.<sup>88</sup> The melting point of the protein is the  $x$ -value of the point of inflection, which is the  $IC_{50}$  value of the logistic function.

#### Antiproliferative assay on HUVECs

HUVECs were procured from Vinod Nursing Home, Bhopal, India; umbilical cord cells were isolated by collagenase treatment of the umbilical cord and HUVECs were further cultured and maintained for all further experiments. [(3-(4,5-Dimethylthiazol-2-yl)-2,5-diphenyltetrazoliumbromide)] or MTT, a pale-yellow substrate, is known to be cleaved by living cells to form a dark blue formazan product. The process involves active mitochondria, and freshly dead cells do not cleave a significant amount of MTT. Hence, the amount of MTT cleaved is in direct proportion with the number of viable cells; this is quantified by colorimetric methods. Test compounds and positive control staurosporine (STS) were solubilized in DMSO and diluted with complete medium to obtain 5 different ranges of test concentrations (10, 1, 0.1, 0.01, and 0.001  $\mu$ M). DMSO concentration was maintained at <0.1% in all the samples. HUVECs maintained in suitable

environments were seeded in 96-well plates and treated with different concentrations of all test compounds and incubated at 37 °C in 5% CO<sub>2</sub> for 96 h. MTT reagents were added to the well plates and kept for incubation for 4 h. The formazan products (dark blue) formed by the living cells were dissolved in DMSO under a safety cabinet and read at 550 nm. The % inhibitions were calculated and IC<sub>50</sub> values for test compounds were determined by plotting the different concentrations used.

#### VEGFR-2 inhibition assay

HUVECs were seeded at 4000–5000 cells per well by using DMEM and 10% FCS for 12 h. Post-incubation, the cells were incubated in serum for 24 h. To the test compound and STS (10 μM), serum was added and incubated for 30 min at 37 °C. The medium was removed, and cells were fixed with 4% formaldehyde in PBS. The cells were washed thrice with PBS. The cells were incubated with anti-phospho VEGF Tyr 1175 antibody (1:1000) for 1 h. The cells were washed thrice with PBS T and incubated with secondary antibody labelled with HRP (1:5000) for 1 h. The cells were washed and incubated with TMB. The reaction was immobilized with 2N H<sub>2</sub>SO<sub>4</sub> and read at 450 nm. The % inhibition was calculated by normalizing with the control.

#### Migration assay

HUVECs were grown to 90% confluency in 6-well plates in DMEM and 10% FCS. A scratch was made with a sterile pipette tip to create a wound. Test compound **14c** and positive control STS 10 μM were added immediately and the cells were imaged. The cells were splashed with 1 mL of DMEM and then with 2 mL of DMEM. They were further incubated at 37 °C in a 5% CO<sub>2</sub> atmosphere. Images were acquired again after 8 h. Cell migration was determined by wound healing (%), which was the distance the cells migrated starting from the original wound margin. Wounds were measured using ImageJ software and % wound closure was calculated and recorded.

#### Capillary tube formation assay

In order to perform capillary-like tube formation assay, HUVECs were trypsinized at 80% confluency and seeded in a 6-well plate at 50 000 cells and DMEM + 10% FCS per well coated with collagen gel. Test compound **14c** and STS in 10 μM concentrations were added at 3 h post seeding and PBS with 0.01% DMSO was used as a control. The plates were incubated at 37 °C in 5% CO<sub>2</sub> for 48 h. The intersections of the tubes were measured in a given field and recorded.

#### MTT cytotoxicity assay

*In vitro* antiproliferative assays were conducted using a procedure previously described.<sup>66,89–91</sup> All the cell lines (MCF-7, K562, A549, and HT-29) were obtained from National Centre for Cell Sciences (NCCS), Pune. To summarize, the

cells were seeded in 96-well flat-bottom micro plates and maintained at 37 °C in 95% humidity and 5% CO<sub>2</sub> overnight. Different concentrations (100, 75, 50, 25, 10, 2.5 μM ml<sup>-1</sup>) of test compound **14c** and positive controls (paclitaxel and cisplatin) were treated. The cells were incubated for 48 h. The wells were washed twice with PBS, 20 μL of MTT staining solution was added to each well and the plate was incubated at 37 °C. After 4 h, 100 μL of DMSO was added to each well to dissolve the formazan crystals, and absorbance was recorded at 570 nm using a microplate reader. The IC<sub>50</sub> of compounds was calculated by using Graph Pad Prism Version 5.1.

Formula:

$$\text{Surviving cells (\%)} = \frac{\text{Mean OD of test compound}}{\text{Mean OD of Negative control}} \times 100$$

#### Molecular docking

Preparation, visualization of structural data and molecular docking were performed using MOE 2019 software (Chemical Computing Group ULC, Canada). The crystal structures of VEGFR-2 (PDB-ID: 1YWN) and HDAC4 (PDB-ID: 4CBY) were obtained from the RCSB Protein Data Bank. The structure files were loaded into the program and subjected to structure preparation including 3D protonation for subsequent docking. The partial charges of all protein and ligand atoms were calculated using the implemented Amber14 force field. Molecular docking was performed choosing the triangle matcher for placement of the ligand in the binding site and ranked with the London dG scoring function. The best 50 poses were passed to the refinement and energy minimization in the pocket using the induced fit method and then rescored using the GBVI/WSA dG scoring function. The protein–ligand complexes were subsequently energy minimized within a radius of 10 Å around the ligand using the Amber14 force field.

#### CAM assay

**Test sample preparation.** Test sample **14c** was submitted in airtight glass vials and stored at 4 °C in a light-controlled environment. A 10 or 1 μg μl<sup>-1</sup> solution of test samples was prepared in PBS and sterilized by passing through a syringe filter (0.22 μm). hVEGF (SIGMA) 50 ng μl<sup>-1</sup> was prepared in sterile PBS.

**Grafting.** Gelatin sponges (Abogel) were cut in approximately 2 mm<sup>3</sup> pieces and loaded with 2 μl of a 1:1 mixture of test substance solution and VEGF solution. The graft was placed on the CAM.

**Eggs.** Fertile hen eggs were procured from a hatchery and were cleaned and decontaminated using alcohol. 1 ml of albumin was removed using a syringe and incubated for 8 days. Grafts were placed on developing CAMs and further incubated to day 12. On day 12, CAMs were fixed with formaldehyde and dissected.

**Imaging.** Fixed CAMs were observed and scored under constant illumination and magnification under a stereomicroscope by two independent experts.

**Statistical analysis.** Data were analyzed on MS Excel 2007.

## Conclusions

In the anticancer drug discovery field, single-targeting agents have failed to show the desired pharmacological effects due to several factors such as intrinsic and acquired resistance. Detailed cellular reports suggest that cancer cells obey Darwin's law of evolution and follow alternative pathways for their survival. Thus, the new strategy to combat drug resistance would be to develop multi-targeting agents endowed with anti-tumor efficacy. Angiogenesis is the fundamental process significant for overall survival of solid tumors; therefore, the search for anti-angiogenic agents has become the primary line of investigation in this field. The epigenetic modulator histone deacetylase has been known to contribute significantly in the progression and metastasis of different cancers. Thus, selecting VEGFR-2 and HDAC would be a rational multi-target approach for the drug discovery of novel chemical weapons to combat cancer.

Herein, we have rationally designed, synthesized, purified, and structurally characterized diaryl-pyrazoline TZD derivatives (nineteen compounds). All the synthetic molecules were primarily screened at 50  $\mu\text{M}$  on two different HDAC isoforms (HDAC4 and HDAC8), which revealed their selectivity towards class II HDAC isoform, *i.e.*, HDAC4, as compared to class I HDAC8. All compounds displayed excellent inhibitory activity on HDAC4 ( $<10 \mu\text{M}$ ) and only a few showed HDAC8 inhibition. Moreover, **13d**, **13j** and **14c** exhibited uncompromised HDAC4  $\text{IC}_{50}$  ( $<1 \mu\text{M}$ ), which suggests that placing a pyrazoline scaffold at the terminal portion and TZD at the ZBG site of the framework was beneficial in enhancing the HDAC potency of the compounds. Based on the results obtained by this study, nine molecules with the best HDAC inhibitory activity were selected to further evaluate their detailed anti-angiogenic capability. These synthesized derivatives were evaluated to determine their effects on HUVEC proliferation, among which **13d**, **14c**, **14d**, and **14j** demonstrated inhibitory activity at  $<10 \mu\text{M}$ , indicating their anti-angiogenic potential. These compounds were further screened at 10  $\mu\text{M}$  on VEGFR-2 which revealed the best compound **14c** with  $>50\%$  VEGFR-2 inhibition and  $\text{IC}_{50}$  of 5  $\mu\text{M}$ . Furthermore, **14c** also possessed an inhibition potential of endothelial cell migration. It was screened on four different cancer cell lines (MCF-7, K562, A549 and HT-29), and it was worth noting that it exhibited anti-proliferative activity on all four cell lines. The anti-angiogenic capability of compound **14c** was further confirmed by an *in vivo* CAM assay which demonstrated significant reduction in the number of capillary branching. Additionally, molecular docking was performed to determine the mechanism of binding mode of **14c** at the VEGFR-2 (PDB ID: 1YWN) and HDAC4 (PDB-ID: 4CBY) receptor sites.

Docking results showed essential binding interactions such as F1045 and D1044 on VEGFR-2, and H842 and F871 on HDAC4.

The results obtained were in agreement with our hypothesis that diaryl-pyrazoline thiazolidinedione analog **14c** holds both anti-angiogenic and HDAC inhibitory activity. To conclude, this study unfolds that **14c** has the potential to simultaneously target both VEGFR-2 and HDAC4. Based on these findings, we put forward that **14c** could be used as a lead for the discovery of more optimized dual inhibitors.

## Conflicts of interest

There are no conflicts of interest to declare.

## Acknowledgements

This research work was supported by an "Indo-ASEAN Collaborative Research Project Grant" from the ASEAN-India S&T Development Fund (AISTDF), Department of Science and Technology (DST), Government of India, Project Reference Number IMRC/AISTDF/CRD/2018/000001 (to CSR); the National Medical Research Council of Singapore (to APK); and the National Medical Research Council of Singapore and the Singapore Ministry of Education under its Research Centres of Excellence Initiative to the Cancer Science Institute of Singapore, National University of Singapore (to APK). We also acknowledge funding through the LOEWE priority program TRABITA, State of Hesse, Germany (to FJMA).

## References

- 1 F. Yang, N. Zhao, D. Ge and Y. Chen, *RSC Adv.*, 2019, **9**, 19571–19583.
- 2 R. Fu, Y. Sun, W. Sheng and D. Liao, *Eur. J. Med. Chem.*, 2017, **136**, 195–211.
- 3 P. Carmeliet and R. K. Jain, *Nature*, 2011, **473**, 298.
- 4 R. S. Kerbel, *N. Engl. J. Med.*, 2008, **358**, 2039–2049.
- 5 N. Ferrara, *Oncology*, 2005, **69**(Suppl 3), 11–16.
- 6 G. Bergers and D. Hanahan, *Nat. Rev. Cancer*, 2008, **8**, 592.
- 7 R. N. Gacche and R. J. Meshram, *Biochim. Biophys. Acta, Rev. Cancer*, 2014, **1846**, 161–179.
- 8 F.-W. Peng, D.-K. Liu, Q.-W. Zhang, Y.-G. Xu and L. Shi, *Expert Opin. Ther. Pat.*, 2017, **27**, 987–1004.
- 9 Y. Li, C. Tan, C. Gao, C. Zhang, X. Luan, X. Chen, H. Liu, Y. Chen and Y. Jiang, *Bioorg. Med. Chem.*, 2011, **19**, 4529–4535.
- 10 N. M. Raghavendra, D. Pingili, S. Kadasi, A. Mettu and S. V. U. M. Prasad, *Eur. J. Med. Chem.*, 2018, **143**, 1277–1300.
- 11 B. D. Smith, M. D. Kaufman, C. B. Leary, B. A. Turner, S. C. Wise, Y. M. Ahn, R. J. Booth, T. M. Caldwell, C. L. Ensinger and M. M. Hood, *Mol. Cancer Ther.*, 2015, **14**, 2023–2034.
- 12 J. Zang, X. Liang, Y. Huang, Y. Jia, X. Li, W. Xu, C. J. Chou and Y. Zhang, *J. Med. Chem.*, 2018, **61**, 5304–5322.
- 13 R. Kurzrock, S. I. Sherman, D. W. Ball, A. A. Forastiere, R. B. Cohen, R. Mehra, D. G. Pfister, E. E. W. Cohen, L. Janisch, F. Nauling, D. S. Hong, C. S. Ng, L. Ye, R. F. Gagel, J. Frye, T.

- Müller, M. J. Ratain and R. Salgia, *J. Clin. Oncol.*, 2011, **29**, 2660–2666.
- 14 K. A. Lyseng-Williamson, *Drugs Ther. Perspect.*, 2018, **34**, 457–465.
- 15 S. Yu, D. Quinn and T. Dorff, *OncoTargets Ther.*, 2016, **9**, 5825–5837.
- 16 T. A. Miller, D. J. Witter and S. Belvedere, *J. Med. Chem.*, 2003, **46**, 5097–5116.
- 17 M. Mottamal, S. Zheng, T. L. Huang and G. Wang, *Molecules*, 2015, **20**, 3898–3941.
- 18 S. Y. Park, J. A. Jun, K. J. Jeong, H. J. Heo, J. S. Sohn, H. Y. Lee, C. G. Park and J. Kang, *Oncol. Rep.*, 2011, **25**, 1677–1681.
- 19 M. Nakagawa, Y. Oda, T. Eguchi, S.-I. Aishima, T. Yao, F. Hosoi, Y. Basaki, M. Ono, M. Kuwano, M. Tanaka and M. Tsuneyoshi, *Oncol. Rep.*, 2007, **18**, 769–774.
- 20 A. Singh, P. Patel, Jageshwar, V. K. Patel, D. K. Jain, M. Kamal and H. Rajak, *Curr. Cancer Drug Targets*, 2018, **18**, 720–736.
- 21 M. Lernoux, M. Schnekenburger, M. Dicato and M. Diederich, *Biochem. Pharmacol.*, 2020, **173**, 113698.
- 22 H. S. Kim, Q. Shen and S. W. Nam, *J. Korean Med. Sci.*, 2015, **30**, 1375–1380.
- 23 Y. Asfaha, C. Schrenk, L. A. Alves Avelar, A. Hamacher, M. Pflieger, M. U. Kassack and T. Kurz, *Bioorg. Med. Chem.*, 2019, **27**, 115087.
- 24 J. L. Guerriero, A. Sotayo, H. E. Ponichtera, J. A. Castrillon, A. L. Pourzia, S. Schad, S. F. Johnson, R. D. Carrasco, S. Lazo, R. T. Bronson, S. P. Davis, M. Lobera, M. A. Nolan and A. Letai, *Nature*, 2017, **543**, 428–432.
- 25 A. Clocchiatti, E. Di Giorgio, G. Viviani, C. Streuli, A. Sgorbissa, R. Picco, V. Cutano and C. Brancolini, *J. Cell Sci.*, 2015, **128**, 3961–3976.
- 26 T. Eckschlager, J. Plch, M. Stiborova and J. Hrabeta, *Int. J. Mol. Sci.*, 2017, **18**, 1414.
- 27 S. Subramanian, S. E. Bates, J. J. Wright, I. Espinoza-Delgado and R. L. Piekarz, *Pharmaceuticals*, 2010, **3**, 2751–2767.
- 28 L. Goracci, N. Deschamps, G. M. Randazzo, C. Petit, C. Dos Santos Passos, P.-A. Carrupt, C. Simões-Pires and A. Nurisso, *Sci. Rep.*, 2016, **6**, 29086.
- 29 S. Shen and A. P. Kozikowski, *ChemMedChem*, 2016, **11**, 15–21.
- 30 T. Suzuki and N. Miyata, *Curr. Med. Chem.*, 2005, **12**, 2867–2880.
- 31 J. S. Kerr, S. Galloway, A. Lagrutta, M. Armstrong, T. Miller, V. M. Richon and P. A. Andrews, *Int. J. Toxicol.*, 2010, **29**, 3–19.
- 32 B. Deng, Q. Luo, A. Halim, Q. Liu, B. Zhang and G. Song, *DNA Cell Biol.*, 2020, **39**, 167–176.
- 33 H. Choudhry, A. L. Harris and A. McIntyre, *Mol. Aspects Med.*, 2016, **47–48**, 35–53.
- 34 K. M. Cook and W. D. Figg, *Ca-Cancer J. Clin.*, 2010, **60**, 222–243.
- 35 M. Friedrich, L. Gerbeth, M. Gerling, R. Rosenthal, K. Steiger, C. Weidinger, J. Keye, H. Wu, F. Schmidt, W. Weichert, B. Siegmund and R. Glauben, *Mucosal Immunol.*, 2019, **12**, 656–667.
- 36 M. Wanjare, S. Kusuma and S. Gerech, *Biotechnol. J.*, 2013, **8**, 434–447.
- 37 W. Gu and R. G. Roeder, *Cell*, 1997, **90**, 595–606.
- 38 M. S. Kim, H. J. Kwon, Y. M. Lee, J. H. Baek, J.-E. Jang, S.-W. Lee, E.-J. Moon, H.-S. Kim, S.-K. Lee and H. Y. Chung, *Nat. Med.*, 2001, **7**, 437.
- 39 L. Chen, J. Li, F. Wang, C. Dai, F. Wu, X. Liu, T. Li, R. Glauben, Y. Zhang, G. Nie, Y. He and Z. Qin, *Cancer Res.*, 2016, **76**, 6828–6838.
- 40 F. Pucci, M. A. Venneri, D. Biziato, A. Nonis, D. Moi, A. Sica, C. Di Serio, L. Naldini and M. De Palma, *Blood*, 2009, **114**, 901–914.
- 41 S. A. Bassett and M. P. Barnett, *Nutrients*, 2014, **6**, 4273–4301.
- 42 I. Hrgovic, M. Doll, A. Pinter, R. Kaufmann, S. Kippenberger and M. Meissner, *Exp. Dermatol.*, 2017, **26**, 194–201.
- 43 H. J. Kwon, M. S. Kim, M. J. Kim, H. Nakajima and K.-W. Kim, *Int. J. Cancer*, 2002, **97**, 290–296.
- 44 M. Michaelis, U. R. Michaelis, I. Fleming, T. Suhan, J. Cinatl, R. A. Blaheta, K. Hoffmann, R. Kotchetkov, R. Busse and H. Nau, *Mol. Pharmacol.*, 2004, **65**, 520–527.
- 45 D. Z. Qian, X. Wang, S. K. Kachhap, Y. Kato, Y. Wei, L. Zhang, P. Atadja and R. Pili, *Cancer Res.*, 2004, **64**, 6626–6634.
- 46 R. Mohan, A. K. Sharma, S. Gupta and C. S. Ramaa, *Med. Chem. Res.*, 2012, **21**, 1156–1165.
- 47 U. Bhanushali, S. Rajendran, K. Sarma, P. Kulkarni, K. Chatti, S. Chatterjee and C. S. Ramaa, *Bioorg. Chem.*, 2016, **67**, 139–147.
- 48 M. McTigue, B. W. Murray, J. H. Chen, Y.-L. Deng, J. Solowiej and R. S. Kania, *Proc. Natl. Acad. Sci. U. S. A.*, 2012, **109**, 18281–18289.
- 49 U. Bhanushali, S. Rajendran, K. Sarma, P. Kulkarni, K. Chatti, S. Chatterjee and C. S. Ramaa, *Bioorg. Chem.*, 2016, **67**, 139–147.
- 50 R. S. K. Vijayan, P. He, V. Modi, K. C. Duong-Ly, H. Ma, J. R. Peterson, R. L. Dunbrack Jr and R. M. Levy, *J. Med. Chem.*, 2014, **58**, 466–479.
- 51 K. M. Kasiotis, E. N. Tzanetou and S. A. Haroutounian, *Front. Chem.*, 2014, **2**(78), DOI: 10.3389/fchem.2014.00078.
- 52 N. Miyamoto, N. Sakai, T. Hirayama, K. Miwa, Y. Oguro, H. Oki, K. Okada, T. Takagi, H. Iwata and Y. Awazu, *Bioorg. Med. Chem.*, 2013, **21**, 2333–2345.
- 53 M. Wang, S. Xu, H. Lei, C. Wang, Z. Xiao, S. Jia, J. Zhi, P. Zheng and W. Zhu, *Bioorg. Med. Chem.*, 2017, **25**, 5754–5763.
- 54 N. Mainolfi, R. Karki, F. Liu and K. Anderson, *ACS Med. Chem. Lett.*, 2016, **7**, 363–367.
- 55 L.-L. Yang, G.-B. Li, S. Ma, C. Zou, S. Zhou, Q.-Z. Sun, C. Cheng, X. Chen, L.-J. Wang, S. Feng, L.-L. Li and S.-Y. Yang, *J. Med. Chem.*, 2013, **56**, 1641–1655.
- 56 A. Sharma, T. Pathan, R. Mohan and C. S. Ramaa, *Lett. Drug Des. Discovery*, 2011, **8**, 843–849.
- 57 D. Havrylyuk, B. Zimenkovsky, O. Vasilenko, A. Gzella and R. Lesyk, *J. Med. Chem.*, 2012, **55**, 8630–8641.
- 58 H. Fahmy, N. Khalifa, M. Ismail, H. El-Sahrawy and E. Nossier, *Molecules*, 2016, **21**, 271.

- 59 G. Nitulescu, C. Draghici and O. Olaru, *Int. J. Mol. Sci.*, 2013, **14**, 21805–21818.
- 60 R. Neelarapu, D. L. Holzle, S. Velaparthi, H. Bai, M. Brunsteiner, S. Y. Blond and P. A. Petukhov, *J. Med. Chem.*, 2011, **54**, 4350–4364.
- 61 J. Wen, Q. Niu, J. Liu, Y. Bao, J. Yang, S. Luan, Y. Fan, D. Liu and L. Zhao, *Bioorg. Med. Chem. Lett.*, 2016, **26**, 375–379.
- 62 J. Yang, G. Cheng, Q. Xu, S. Luan, S. Wang, D. Liu and L. Zhao, *Bioorg. Med. Chem.*, 2018, **26**, 1418–1425.
- 63 C. Zagni, A. Citarella, M. Oussama, A. Rescifina, A. Maugeri, M. Navarra, A. Scala, A. Piperno and N. Micale, *Int. J. Mol. Sci.*, 2019, **20**, 945.
- 64 D. T. Hieu, D. T. Anh, N. M. Tuan, P.-T. Hai, L.-T.-T. Huong, J. Kim, J. S. Kang, T. K. Vu, P. T. P. Dung, S.-B. Han, N.-H. Nam and N.-D. Hoa, *Bioorg. Chem.*, 2018, **76**, 258–267.
- 65 S. Minucci and P. G. Pelicci, *Nat. Rev. Cancer*, 2006, **6**, 38–51.
- 66 K. Tilekar, N. Upadhyay, N. Jänsch, M. Schweipert, P. Mrowka, F. J. Meyer-Almes and C. S. Ramaa, *Bioorg. Chem.*, 2020, **95**, 103522.
- 67 N. Upadhyay, K. Tilekar, N. Jänsch, M. Schweipert, J. D. Hess, L. Henze Macias, P. Mrowka, R. J. Aguilera, J. Choe, F.-J. Meyer-Almes and C. S. Rama, *Bioorg. Chem.*, 2020, 103934.
- 68 K. Tilekar, J. D. Hess, N. Upadhyay, A. L. Bianco, M. Schweipert, A. Laghezza, F. Loiodice, F.-J. Meyer-Almes, R. J. Aguilera, A. Lavecchia and R. C. S., *J. Med. Chem.*, 2021, **64**, 6949–6971.
- 69 K. Tilekar, N. Upadhyay, J. D. Hess, L. H. Macias, P. Mrowka, R. J. Aguilera, F.-J. Meyer-Almes, C. V. Iancu, J.-Y. Choe and C. S. Ramaa, *Eur. J. Med. Chem.*, 2020, **202**, 112603.
- 70 P. Tessier, D. V. Smil, A. Wahhab, S. Leit, J. Rahil, Z. Li, R. Déziel and J. M. Besterman, *Bioorg. Med. Chem. Lett.*, 2009, **19**, 5684–5688.
- 71 R. W. Bürli, C. A. Luckhurst, O. Aziz, K. L. Matthews, D. Yates, Kathy. A. Lyons, M. Beconi, G. McAllister, P. Breccia, A. J. Stott, S. D. Penrose, M. Wall, M. Lamers, P. Leonard, I. Müller, C. M. Richardson, R. Jarvis, L. Stones, S. Hughes, G. Wishart, A. F. Haughan, C. O'Connell, T. Mead, H. McNeil, J. Vann, J. Mangette, M. Maillard, V. Beaumont, I. Munoz-Sanjuan and C. Dominguez, *J. Med. Chem.*, 2013, **56**, 9934–9954.
- 72 C. A. Luckhurst, O. Aziz, V. Beaumont, R. W. Bürli, P. Breccia, M. C. Maillard, A. F. Haughan, M. Lamers, P. Leonard, K. L. Matthews, G. Raphy, A. J. Stott, I. Munoz-Sanjuan, B. Thomas, M. Wall, G. Wishart, D. Yates and C. Dominguez, *Bioorg. Med. Chem. Lett.*, 2019, **29**, 83–88.
- 73 R. W. Bürli, C. A. Luckhurst, O. Aziz, K. L. Matthews, D. Yates, Kathy. A. Lyons, M. Beconi, G. McAllister, P. Breccia, A. J. Stott, S. D. Penrose, M. Wall, M. Lamers, P. Leonard, I. Müller, C. M. Richardson, R. Jarvis, L. Stones, S. Hughes, G. Wishart, A. F. Haughan, C. O'Connell, T. Mead, H. McNeil, J. Vann, J. Mangette, M. Maillard, V. Beaumont, I. Munoz-Sanjuan and C. Dominguez, *J. Med. Chem.*, 2013, **56**, 9934–9954.
- 74 M. Adel, R. A. T. Serya, D. S. Lasheen and K. A. M. Abouzid, *Bioorg. Chem.*, 2018, **81**, 612–629.
- 75 H.-J. Park, Y. Zhang, S. P. Georgescu, K. L. Johnson, D. Kong and J. B. Galper, *Stem Cell Rev.*, 2006, **2**, 93–101.
- 76 A. M. Goodwin, *Microvasc. Res.*, 2007, **74**, 172–183.
- 77 C. A. Staton, M. W. R. Reed and N. J. Brown, *Int. J. Exp. Pathol.*, 2009, **90**, 195–221.
- 78 D. Y. Kim, J. A. Park, Y. Kim, M. Noh, S. Park, E. Lie, E. Kim, Y. Kim and Y. Kwon, *FASEB J.*, 2019, **33**, 9842–9857.
- 79 Q. Zhang, S. Lu, T. Li, L. Yu, Y. Zhang, H. Zeng, X. Qian, J. Bi and Y. Lin, *J. Exp. Clin. Cancer Res.*, 2019, **38**, 173.
- 80 J. Li, X. Sun, Z. Wang, L. Chen, D. Li, J. Zhou and M. Liu, *PLoS One*, 2012, **7**, e36389.
- 81 Z. Li, C. Zhu, B. An, Y. Chen, X. He, L. Qian, L. Lan and S. Li, *Oncotargets Ther.*, 2018, **11**, 2937–2944.
- 82 K. Tilekar, N. Upadhyay, F. Meyer-Almes, F. Loiodice, N. Y. Anisimova, T. S. Spirina, D. V. Sokolova, G. B. Smirnova, J. Choe, V. S. Pokrovsky, A. Lavecchia and C. S. Ramaa, *ChemMedChem*, 2020, **15**, 1813–1825.
- 83 N. Upadhyay, K. Tilekar, F. Loiodice, N. Yu. Anisimova, T. S. Spirina, D. V. Sokolova, G. B. Smirnova, J. Choe, F.-J. Meyer-Almes, V. S. Pokrovsky, A. Lavecchia and C. S. Ramaa, *Bioorg. Chem.*, 2020, 104527.
- 84 U. Bhanushali, S. Rajendran, K. Sarma, P. Kulkarni, K. Chatti, S. Chatterjee and C. S. Ramaa, *Bioorg. Chem.*, 2016, **67**, 139–147.
- 85 V. Patil, K. Tilekar, S. Mehendale-Munj, R. Mohan and C. S. Ramaa, *Eur. J. Med. Chem.*, 2010, **45**, 4539–4544.
- 86 N. Jänsch, C. Meyners, M. Muth, A. Kopranovic, O. Witt, I. Oehme and F.-J. Meyer-Almes, *Redox Biol.*, 2019, **20**, 60–67.
- 87 B. Wolff, N. Jänsch, W. O. Sugiarto, S. Frühschulz, M. Lang, R. Altintas, I. Oehme and F.-J. Meyer-Almes, *Eur. J. Med. Chem.*, 2019, **184**, 111756.
- 88 A. Volund, *Biometrics*, 1978, **34**, 357.
- 89 M. R. Peram, S. Jalalpure, V. Kumbhar, S. Patil, S. Joshi, K. Bhat and P. Diwan, *J. Liposome Res.*, 2019, 1–21.
- 90 N. Upadhyay, K. Tilekar, N. Jänsch, M. Schweipert, J. D. Hess, L. Henze Macias, P. Mrowka, R. J. Aguilera, J. Choe, F.-J. Meyer-Almes and C. S. Rama, *Bioorg. Chem.*, 2020, 103934.
- 91 K. Tilekar, N. Upadhyay, M. Schweipert, J. D. Hess, L. H. Macias, P. Mrowka, F.-J. Meyer-Almes, R. J. Aguilera, C. V. Iancu, J.-Y. Choe and C. S. Ramaa, *Eur. J. Pharm. Sci.*, 2020, **154**, 105512.